Robust topological surface state in Kondo insulator SmB6 thin films

Jie Yong, Yeping Jiang, Demet Usanmaz, Stefano Curtarolo, Xiaohang Zhang, Linze Li, Xiaoqing Pan, Jongmoon Shin, Ichiro Takeuchi, and Richard L. Greene

Citation: Applied Physics Letters **105**, 222403 (2014); doi: 10.1063/1.4902865
View online: http://dx.doi.org/10.1063/1.4902865
View Table of Contents: http://scitation.aip.org/content/aip/journal/apl/105/22?ver=pdfcov
Published by the AIP Publishing

Robust topological surface state in Kondo insulator SmB_6 thin films

Jie Yong,[1,2,a)] Yeping Jiang,[1,2] Demet Usanmaz,[3] Stefano Curtarolo,[3] Xiaohang Zhang,[1,2] Linze Li,[4] Xiaoqing Pan,[4] Jongmoon Shin,[5] Ichiro Takeuchi,[1,5] and Richard L. Greene[1,2]
[1]*Center for Nanophysics and Advanced Materials, University of Maryland, College Park, Maryland 20742, USA*
[2]*Department of Physics, University of Maryland, College Park, Maryland 20742, USA*
[3]*Department of Mechanical Engineering and Materials Science, Duke University, Durham, North Carolina 27708, USA*
[4]*Department of Materials Science and Engineering, University of Michigan, Ann Arbor, Michigan 48109, USA*
[5]*Department of Materials Science and Engineering, University of Maryland, College Park, Maryland 20742, USA*

(Received 18 October 2014; accepted 15 November 2014; published online 1 December 2014)

Fabrication of smooth thin films of topological insulators with true insulating bulk are extremely important for utilizing their novel properties in quantum and spintronic devices. Here, we report the growth of crystalline thin films of SmB_6, a topological Kondo insulator with true insulating bulk, by co-sputtering both SmB_6 and B targets. X-ray diffraction, Raman spectroscopy, and transmission electron microscopy indicate films that are polycrystalline with a (001) preferred orientation. When cooling down, resistivity ρ shows an increase around 50 K and saturation below 10 K, consistent with the opening of the hybridization gap and surface dominated transport, respectively. The ratio ρ_{2K}/ρ_{300K} is only about two, much smaller than that of bulk, which indicates a much larger surface-to-bulk ratio. Point contact spectroscopy using a superconductor tip on SmB_6 films shows both a Kondo Fano resonance and Andeev reflection, indicating an insulating Kondo lattice with metallic surface states. © *2014 AIP Publishing LLC*.
[http://dx.doi.org/10.1063/1.4902865]

Topological insulators (TIs) are a class of promising materials, which have insulating bulk but protected conducting surfaces due to the combination of spin-orbit interactions and time-reversal symmetry. The surface states are topologically non-trivial and robust against non-magnetic backscattering, leading to fascinating physics and potential false-tolerant quantum computing applications.[1,2] However, the bulk of most topological insulators found so far, such as Bi_2Se_3 and Bi_2Te_3, are not insulating due to lattice vacancies or self-doping.[3] Even in highest-quality samples of topological insulators, in which the presence of vacancies is negligible as well as the surface is stable and chemically inert,[4] the Fermi level is at the bottom of the conduction band.[5] This makes it difficult to utilize the surface properties of TIs because a conducting bulk complicates the topological surface transport. The prediction and discovery of SmB_6 as a topological insulator[6,7] is extremely exciting because it has a truly insulating bulk state. Moreover, it is well known that SmB_6 is also a Kondo insulator which means there will be interesting interplay between correlated physics and topological properties. The fundamental step of utilizing these topological and correlated properties in actual devices requires us prepare SmB_6 in thin film form. Here, we report the fabrication of smooth thin films of nanocrystalline SmB_6 and show that their transport behavior indeed indicates that SmB_6 is a bulk insulator with topological surface states. Point contact spectroscopy (PCS) of the films using a superconducting tip displays both a Kondo Fano resonance and Andreev reflection, suggesting the existence of both an insulating Kondo lattice and metallic surface states.

Upon decreasing the temperature, the resistivity of SmB_6 increases like an insulator but saturates at temperatures below 5 K.[8–18] Recent transport measurements show that the resistance of this saturation is thickness-independent for both longitudinal and transverse directions.[11–13] Moreover, weak anti-localization and linear magnetoresistance have been observed in single crystal SmB_6 to support the presence of spin-momentum locked surface states.[14] It has been shown that doping SmB_6 with magnetic impurities diminishes this saturation, while non-magnetic impurities do not.[12] These facts suggest that the conduction is from the surface state; it is protected by time-reversal symmetry, and is robust against non-magnetic scatterings. Quantum oscillations of the surface states have been observed by torque magnetometry measurements[19] and the tracking of the Landau levels in the infinite magnetic field limit points to $-1/2$, which indicates a 2D Dirac electronic state. Neutron[20,21] and surface sensitive measurements, such as angle resolved photoemission (ARPES)[22–29] and scanning tunneling microscopy[30–32] (STM), confirm the formation of the hybridization gap and the existence of the surface states. One study,[28] in particular, suggests that the surface states are spin polarized with spin momentum locking which is a signature of the topological states. Unfortunately, there are also reports that indicate the resistivity saturation is due to dangling surface bonds[25] or complicated by carbon impurities.[33] Preparation of SmB_6 in thin film geometries with smooth surfaces can facilitate device patterning, heterostructures fabrication, and surface sensitive measurements that will give direct insight on the topological nature of this material and lay a foundation on building quantum or spintronic devices on this material. In particular, smooth thin films would allow fabrication of heterostructures for probing the long-

a)Email: jyong@umd.edu

sought Majorana fermions by coupling SmB_6 with a conventional superconductor.[34]

We initially attempted growth of SmB_6 thin films via pulsed laser deposition and sputtering using single SmB_6 targets, but these growths resulted in grossly boron deficient films. In order to achieve the correct stoichiometry, we turned to the combinatorial composition-spread approach by co-sputtering of SmB_6 and boron targets.[35] By covering a large range of continuous average composition on a given spread wafer, this method can be used to ensure that somewhere on the wafer, there is a region with the correct average stoichiometry. SmB_6 and B targets were co-sputtered at dc 50 W and rf 100 W, respectively, in a high-vacuum combinatorial co-sputtering chamber. Boron is brittle and insulating, and its deposition rate is much lower than that of the SmB_6 target. The base pressure of the deposition chamber is typically 2×10^{-8} Torr. The substrates used were MgO and 3-in. (001) oriented Si wafers with a 300 nm amorphous SiO_2 layer. Films on different substrates show consistent behavior. A physical shadow mask is placed over the wafer during the deposition to naturally separate the film into 2 mm × 2 mm squares. The typical argon pressure was 6.5 mTorr during the deposition, and the substrate was heated at 800 °C during the deposition and for 3 h following the deposition in vacuum. The deposition thickness across the spread varied from 80 to 200 nm.

The composition variation of the Sm_xB_{1-x} spreads is mapped by wavelength dispersive spectroscopy (WDS), with an error bar of about 1%. Fig. 1(a) plots the composition of Sm(x) mapped across a typical spread: it runs from about 0.01 directly underneath the B target to about 0.34 underneath the SmB_6 target. The desired composition of SmB_6 ($x = 0.14$) is obtained in the middle of the spread wafer. X-ray diffraction (XRD) of the spread is carried out with an area detector (Vantec500) using a Bruker D8 Discover with the CuKα line. Fig. 1(b) shows the X-ray diffraction pattern (integrated in the chi direction) from the part of the spread film whose composition is SmB_6. A broad ring was seen in the area detector (not shown), which indicates the highly polycrystalline nature of the film. The pattern indicates that the film is preferentially oriented in the (001) direction, but peaks from other orientations, such as (011) and (021), are also present. Upon scanning XRD across the entire range ($0.01 \leq \times \leq 0.34$), we found that the predominant phase in the composition spread is always SmB_6, regardless of x (not shown). This is surprising because there are reports of several other intermetallic phases,[36,37] such as SmB_4 and Sm_2B_5, whose samarium stoichiometry is within the deposition range.

To address this, we performed quantum mechanical parameterization of the Sm-B system to understand the phase formation and stability within the AFLOWLIB framework[38,39] using the standard computational parameters as specified in Ref. 40. Fig. 2 shows, in blue line, the minimum formation free energy (E_f) at zero temperature. Based on the calculations, the low temperature thermodynamics would indeed dictate that the first precipitating phase should be SmB_4, having the minimum formation energy E_f in the entire composition range, since E_f represents the strength of the system to oppose phase separation. However, due to the hyper-thermal plasma process of sputtering, the Sm-B feedstock solution in the vapor phase starts off with an extremely large amount of intrinsic entropy (from translational degrees of freedom of vapor), and as a result, the entropic temperature T_s of a compound (a measure of the entropy to overcome the formation energy) emerges as the key factor which determines the strength of the system to compensate for the entropy of the feedstock.[40,41] Given the locations of phases in Figure 2, one sees that, from the point of view of the

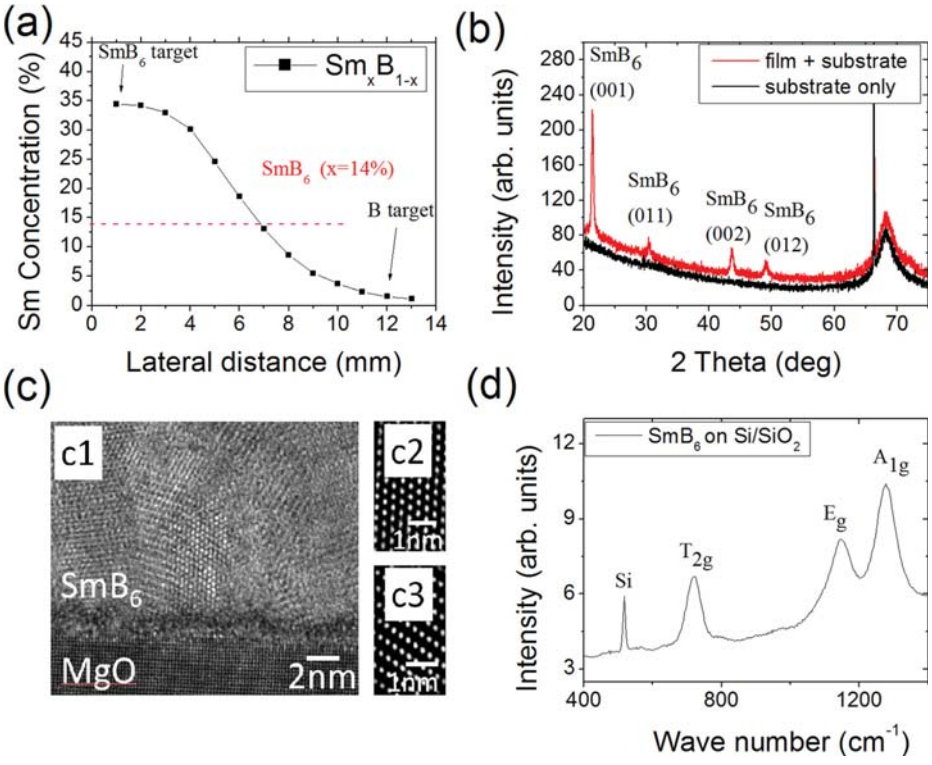

FIG. 1. The fabrication and characterization of SmB_6. (a) Samarium concentration x, measured by WDS, as function of lateral distance. (b) Integrated X-ray diffraction intensity with areal detector for the film with the substrate (in red) and with only the substrate (in black). The substrate is 300 nm SiO_2 on Si wafer. (c) Cross-sectional TEM image on the interface between SmB_6 film and MgO substrate. (c1) raw image revealing textured structures with amorphous areas. (c2) and (c3) are selected areas after filtering showing SmB_6 (011) and (111) planes. (d), Raman spectrum of SmB_6 films on Si/SiO_2 substrate. The laser wavelength used is 532 nm. Three modes T_{2g}, E_g, and A_{1g} from SmB_6 are clearly seen.

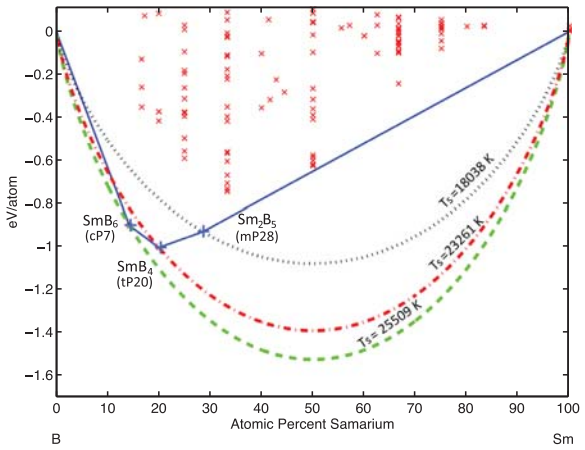

FIG. 2. Free energy convex hull for B-Sm at zero temperature (solid blue line). Blue/red crosses indicate stable/unstable phases. Space groups are in parentheses below the stable compound stoichiometries. The three dashed curves indicate the entropic temperature envelopes.[36,37] Cooling from the hyper-thermal plasma of sputtering, it is actually SmB_6 with the highest T_s which nucleates first.

vapor, the most "accommodating" phase to nucleate is actually SmB_6 with its highest relative T_s compared to the other phases. This follows from the fact that during nucleation, the entropy maximization will limit the flow of latent heat and therefore chooses the phase most capable of accepting and transforming entropy (from translational to configurational). Thus, the non-equilibrium nature of the co-sputtering process has served as the key enabler which allowed us to achieve the desired SmB_6 phase in the present synthesis method.

To further confirm the existence of SmB_6, we performed cross sectional transmission electron microscopy (TEM) and Raman spectroscopy on films with x near 0.14. Fig. 1(c) shows the high resolution cross sectional TEM images of films on a MgO substrate. Nanocrystalline SmB_6 grains with different orientations can be clearly seen. Figs. 1(c2) and 1(c3) show the enlarged images (after filtering) of two selected grains with (011) and (111) orientations, respectively. The lattice constant determined from the image is 4.14 Å, which is consistent with that of the reported bulk value. We also performed Atomic Force Microscopy (AFM) on our films and the typical rms roughness is less than 1.0 nm for a 20 μm by 20 μm area (not shown).

Raman spectrum of a SmB_6 film on Si substrate is done in a Horiba Jobin Yvon LabRam ARAMIS spectrometer using a 532 nm wavelength laser. The result is shown in Fig. 1(d). Three modes T_{2g}, E_g, and A_{1g} from SmB_6 (cubic structure with the Pm3m symmetry) are seen in addition to the Si substrate peak at 510 cm^{-1}.[42] The wavenumbers of these three peaks are consistent with those from the single crystals. They are first order Raman modes which involve the displacement of the boron octahedral. The Sm ion is at a site of inversion symmetry and cannot contribute to first order phonon Raman scattering. The fact that the widths of these three peaks are wider than the Si substrate peak also indicates that these films are polycrystalline.

Transport and point contact spectroscopy measurements are done in a Quantum Design Physical Property Measurement System (PPMS). Sheet resistance is measured in four point Van der Pauw configurations. Contacts are made by a wire bonder using Al wires. Sheet resistance is calculated by $R_s = V\ \pi/(I\ \ln 2)$. Resistivity is calculated by $\rho = R_s\ t$ (thickness of the film). We have carefully extracted different sections of the spread film with different compositions to carry out resistivity measurements. The sheet resistance R_s (Fig. 3, left axis) and resistivity ρ (Fig. 3, right axis) vs temperature curves are plotted for three different boron concentration films with thickness about 100 nm. We use sheet resistance here since at low temperatures the measured resistance arises from the surface state as discussed below. Comparing the three concentrations ($x = 0.10$, 0.14, and 0.22), the room temperature resistivity $\rho(300\,K)$ increases with increasing boron concentration. At 300 K, a typical resistivity for a stoichiometric SmB_6 film is around 300 $\mu\Omega$ cm, which is similar to that of bulk SmB_6 crystals.[1,2,16,19]

For single SmB_6 crystals, though the proposed topological property is yet to be verified, the bulk insulating and surface conductive nature have been established.[11–14] Our films show similar behaviors. As the temperature is decreased, all three films show increase in the resistivity with a particularly rapid rise below 50 K. This behavior is consistent with the opening of the hybridization gap between the itinerant 5d band and localized Sm 4f band as found in bulk SmB_6 crystals.[8–10] Below 10 K, the sheet resistance displays a saturating behavior for the film with $x > 0.10$, but it continues to increase for the $x < 0.10$ sample. The saturation behavior, regarded as a mystery for decades, is now widely accepted as the signature of the emergence of the conducting surface state. We note that our saturated sheet resistance ($R_s \sim 50\ \Omega$ at 2 K) is very close to the reported sheet resistance of single crystals at low temperatures.[12] If the low temperature conduction is from the bulk of the film, one would expect a much larger sheet resistance because the films are three orders of magnitude thinner than typical crystals. Also if the conduction is from some trivial surface state, one would expect a very large sheet resistance due to grain boundary scattering because our films are nanocrystalline. The fact that we observe a very similar sheet resistance strongly supports that this low temperature conduction is from the surface and that this surface conduction is protected against

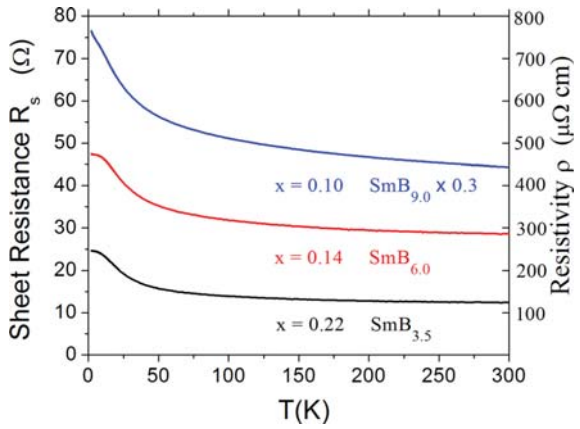

FIG. 3. Temperature dependences of sheet resistances (left axis) and resistivities (right axis) for three Sm_xB_{1-x} films with $x = 0.10$, 0.16, and 0.22, respectively. The films are about 100 nm thick and resistances are measured using the Van Der Pauw method.

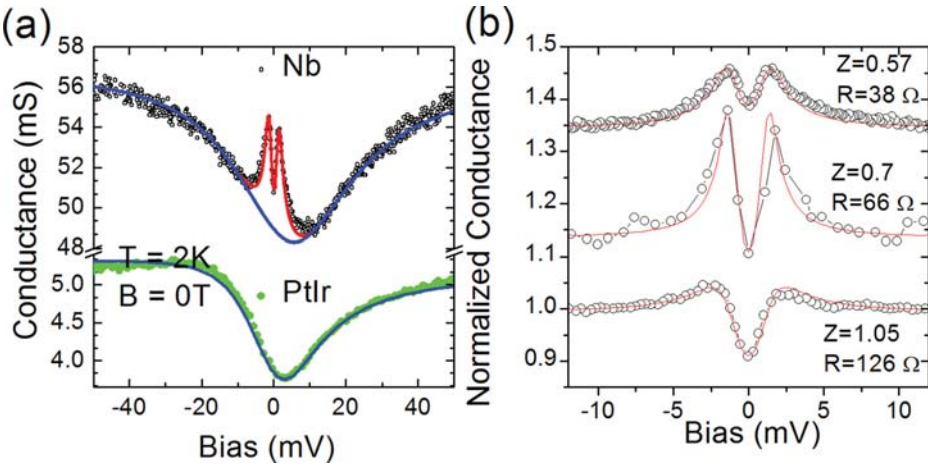

FIG. 4. PCS on SmB_6 films. (a) PCS on the SmB_6 film with a PtIt tip (green filled squares) and a superconducting Nb tip (black open circles). The blue curves are the best fittings to the Fano line shape. The red curve is the fitting to both Fano line shape and modified BTK model. (b) Andreev reflection data (black open circles, all data are normalized to their high bias values and vertically shifted for clarity purposes) of different Nb/SmB_6 junction resistances. Fano background is subtracted. The red curves are the fitting to the BTK model. The spectra here were taken at 2 K and in zero magnetic field.

conventional grain-boundary scatterings. This agrees with the predicted nontrivial nature of the surface states in SmB_6, in which the topologically protected surface states exist only at the interfaces between materials of different topology. Thus, the similar and robust surface conduction in our polycrystalline SmB_6 films compared to single crystals strongly supports the topological aspect of the surface states.

The resistivity ratio between 300 K and 2 K is about 1.7, which is substantially lower than that found in single crystals, where the ratio can be as large as 10^4. This can be explained by a much larger surface to bulk conduction ratio for films. It has indeed been shown that when single crystals are thinned down from 200 μm to 37.5 μm, this ratio ρ_{2K}/ρ_{300K} decreases from 10^4 to less than 3000. A detailed study[18] has shown that the ratio has roughly a linear dependence on the thickness. Given the ratio value of 1.7, an extrapolation of this linear dependence gives a thickness of 242 nm, which is of the order of our film thickness ($\sim$100 nm). Of course, this linear relationship might not be valid down to 100 nm, but this rough agreement with the linear thickness dependence demonstrates that our thin films are already in a limit, where the surface conduction at lowest temperature is comparable to the bulk conduction at room temperature. Therefore, we attribute the saturation and the small resistance increase in our films to the surface conducting state.

The Kondo nature of SmB_6 can be investigated by PCS.[14] Fig. 4(a) (the bottom curve) shows a typical PCS curve of our SmB_6 films with a PtIr tip, exhibiting an asymmetric Fano line shape.[43,44] When a superconducting Nb tip is used for the contact (the top curve of Fig. 4(a)), inside the Fano dip and around the Fermi level a clear double peak feature appears, indicating the emergence of Andreev reflection, which takes place in a metal-superconductor junction. The fitting to the Fano line shape (blue curves) gives a Kondo gap of around 19 meV, which is similar to that observed in single crystals.[14] The red curve is the best fit to the Fano line shape and the Blonder-Tinkham-Klapwijk (BTK) model,[45] which gives $\Delta = 1.35$ meV, $Z = 0.57$ (barrier strength), and $\Gamma = 1.0$ meV (broadening term). The gap value is consistent with that of Nb, and above its T_c, the spectrum only shows a Fano line shape with no Andreev enhancement. When the point contact force is varied, the barrier strength (Z) of the junction decreases with junction resistance, while clear signature of the superconducting gap remains, as shown in Fig. 4(b). The co-occurrence of the Kondo feature and Andreev reflection in the SmB_6-superconductor junction clearly signifies the Kondo nature and the simultaneous existence of metallic states at the Fermi level in our films, which, although polycrystalline, reinforces the theoretical prediction that SmB_6 is a topological Kondo insulator. The observation of Andreev reflection implies that high transparency can be achieved in the superconductor/SmB_6 interface.

In summary, we fabricated polycrystalline SmB_6 films by combinatorial sputtering. XRD, TEM, and Raman studies indicate the films are polycrystalline with a (001) preferred orientation. Transport measurements confirmed the presence of a conducting surface state for films which results in the low temperature saturation of the sheet resistance and a small resistance ratio between 2 K and 300 K. PCS using a superconducting tip confirmed the co-existence of a Kondo lattice and a metallic surface state by observation of both the Fano resonance and Andreev reflection. These results are all consistent with SmB_6 being a topological Kondo insulator. Synthesis of SmB_6 thin films with true bulk insulation is an important step towards pursuing proximity induced topological superconductivity in SmB_6 and making devices for quantum computing.

The authors acknowledge fruitful discussions with V. Galitski at the University of Maryland, and T. Mcqueen at John Hopkins University. This work was supported by ONR N00014-13-1-0635 and NSF DMR 1410665. I.T. and S.C. also acknowledge support by the Duke University Center for Materials Genomics.

[1]X. L. Qi and S. C. Zhang, Rev. Mod. Phys. **83**, 1057 (2011).
[2]M. Hasan and C. Kane, Rev. Mod. Phys. **82**, 3045 (2010).
[3]Y. Ando, J. Phys. Soc. Jpn. **82**, 102001 (2013).
[4]A. Politano, M. Caputo, S. Nappini, F. Bondino, E. Magnano, Z. S. Aliev, M. B. Babanly, A. Goldoni, G. Chiarello, and E. V. Chulkov, J. Phys. Chem. C **118**, 21517 (2014).
[5]J. G. Analytis, J.-H. Chu, Y. Chen, F. Corredor, R. D. McDonald, Z. X. Shen, and I. R. Fisher, Phys. Rev. B **81**, 205407 (2010).
[6]M. Dzero, K. Sun, V. Galitski, and P. Coleman, Phys. Rev. Lett. **104**, 106408 (2010).
[7]F. Lu, J. Zhao, H. Weng, Z. Fang, and X. Dai, Phys. Rev. Lett. **110**, 096401 (2013).

[8]J. C. Nickerson, R. M. White, K. N. Lee, R. Bachmann, T. H. Geballe, and G. W. Hull, Jr., Phys. Rev. B **3**, 2030 (1971).
[9]J. W. Allen, B. Batlogg, and P. Wachter, Phys. Rev. B **20**, 4807 (1979).
[10]J. C. Cooley, M. C. Aronson, Z. Fisk, and P. C. Canfield, Phys. Rev. Lett. **74**, 1629 (1995).
[11]D. J. Kim, S. Thomas, T. Grant, J. Botimer, Z. Fisk, and Jing Xia, Sci. Rep. **3**, 3150 (2013).
[12]D. J. Kim, J. Xia, and Z. Fisk, Nat. Mater. **13**, 466 (2014).
[13]S. Wolgast, Ç. Kurdak, K. Sun, J. W. Allen, D. J. Kim, and Z. Fisk, Phys. Rev. B **88**, 180405(R) (2013).
[14]X. Zhang, N. P. Butch, P. Syers, S. Ziemak, R. L. Greene, and J. Paglione, Phys. Rev. X **3**, 011011 (2013).
[15]S. Thomas, D. J. Kim, S. B. Chung, T. Grant, Z. Fisk, and J. Xia, e-print arXiv:1307.4133.
[16]Y. Nakajima, P. Syers, X. F. Wang, R. X. Wang, and J. Paglione, e-print arXiv:1312.6132.
[17]F. Chen, C. Shang, A. F. Wang, X. G. Luo, T. Wu, and X. H. Chen, e-print arXiv:1309.2378.
[18]P. Syers, D. Kim, M. S. Fuhrer, and J. Paglione, e-print arXiv:1408.3402.
[19]G. Li, Z. Xiang, F. Yu, T. Asaba, B. Lawson, P. Cai, C. Tinsman, A. Berkley, S. Wolgast, Y. S. Eo, D. J. Kim, C. Kurdak, J. W. Allen, K. Sun, X. H. Chen, Y. Y. Wang, Z. Fisk, and Lu Li, e-print arXiv:1306.5221.
[20]W. T. Fuhrman, J. Leiner, P. Nikolić, G. E. Granroth, M. B. Stone, M. D. Lumsden, L. DeBeer-Schmitt, P. A. Alekseev, J.-M. Mignot, S. M. Koohpayeh, P. Cottingham, W. Adam Phelan, L. Schoop, T. M. McQueen, and C. Broholm, e-print arXiv:1407.2647.
[21]W. T. Fuhrman and P. Nikolic, e-print arXiv:1409.3220.
[22]J. Jiang, S. Li, T. Zhang, Z. Sun, F. Chen, Z. R. Ye, M. Xu, Q. Q. Ge, S. Y. Tan, X. H. Niu, M. Xia, B. P. Xie, Y. F. Li, X. H. Chen, H. H. Wen, and D. L. Feng, Nat. Commun. **4**, 3010 (2013).
[23]M. Neupane, N. Alidoust, S. Y. Xu, T. Kondo, Y. Ishida, D. J. Kim, C. Liu, I. Belopolski, Y. J. Jo, T. R. Chang, H. T. Jeng, T. Durakiewicz, L. Balicas, H. Lin, A. Bansil, S. Shin, Z. Fisk, and M. Z. Hasan, Nat. Commun. **4**, 2991 (2013).
[24]J. D. Denlinger, J. W. Allen, J.-S. Kang, K. Sun, J.-W. Kim, J. H. Shim, B. I. Min, D.-J. Kim, and Z. Fisk, e-print arXiv:1312.6637v2.
[25]Z.-H. Zhu, A. Nicolaou, G. Levy, N. P. Butch, P. Syers, X. F. Wang, J. Paglione, G. A. Sawatzky, I. S. Elfimov, and A. Damascelli, Phys. Rev. Lett. **111**, 216402 (2013).
[26]N. Xu, X. Shi, P. K. Biswas, C. E. Matt, R. S. Dhaka, Y. Huang, N. C. Plumb, M. Radovic, J. H. Dil, E. Pomjakushina, A. Amato, Z. Salman, D. McK. Paul, J. Mesot, H. Ding, and M. Shi, Phys. Rev. B **88**, 121102(R) (2013).
[27]E. Frantzeskakis, N. de Jong, B. Zwartsenberg, Y. K. Huang, Y. Pan, X. Zhang, J. X. Zhang, F. X. Zhang, L. H. Bao, O. Tegus, A. Varykhalov, A. de Visser, and M. S. Golden, Phys. Rev. X **3**, 041024 (2013).
[28]N. Xu, P. K. Biswas, J. H. Dil, R. S. Dhaka, G. Landolt, S. Muff, C. E. Matt, X. Shi, N. C. Plumb, M. Radovic, E. Pomjakushina, K. Conder, A. Amato, S. V. Borisenko, R. Yu, H.-M. Weng, Z. Fang, X. Dai, J. Mesot, H. Ding, and M. Shi, Nat. Commun. **5**, 4566 (2014).
[29]N. Xu, C. E. Matt, E. Pomjakushina, X. Shi, R. S. Dhaka, N. C. Plumb, M. Radović, P. K. Biswas, D. Evtushinsky, V. Zabolotnyy, J. H. Dil, K. Conder, J. Mesot, H. Ding, and M. Shi, Phys. Rev. B **90**, 085148 (2014).
[30]W. Ruan, C. Ye, M. Guo, F. Chen, X. Chen, G. Zhang, and Y. Wang, Phys. Rev. Lett. **112**, 136401 (2014).
[31]M. M. Yee, Y. He, A. Soumyanarayanan, D.-J. Kim, Z. Fisk, and J. E. Hoffman, e-print arXiv:1308.1085.
[32]S. Rößler, T. H. Jang, D. J. Kim, L. H. Tjeng, Z. Fisk, F. Steglich, and S. Wirth, Proc. Natl. Acad. Sci. U.S.A. **111**, 4798 (2014).
[33]W. A. Phelan, S. M. Koohpayeh, P. Cottingham, J. W. Freeland, J. C. Leiner, C. L. Broholm, and T. M. McQueen, Phys. Rev. X **4**, 031012 (2014).
[34]L. Fu and C. L. Kane, Phys. Rev. Lett. **100**, 096407 (2008).
[35]K. Jin, R. Suchoski, S. Fackler, Y. Zhang, X. Q. Pan, R. L. Greene, and I. Takeuchi, APL Mater. **1**, 042101 (2013).
[36]T. B. Massalski, *Binary Alloy Phase Diagrams* (American Society for Metals, Materials Park, OH, 1990).
[37]P. Villars, M. Berndt, K. Brandenburg, K. Cenzual, J. Daams, F. Hulliger, T. Massalski, H. Okamoto, K. Osaki, A. Prince, H. Putz, and S. Iwata, J. Alloys Compd. **367**, 293 (2004).
[38]S. Curtarolo, W. Setyawan, G. L. W. Hart, M. Jahnatek, R. V. Chepulskii, R. H. Taylor, S. Wang, J. Xue, K. Yang, O. Levy, M. Mehl, H. T. Stokes, D. O. Demchenko, and D. Morgan, Comput. Mater. Sci. **58**, 218 (2012).
[39]S. Curtarolo, W. Setyawan, S. Wang, J. Xue, K. Yang, R. H. Taylor, L. J. Nelson, G. L. W. Hart, S. Sanvito, M. B. Nardelli, N. Mingo, and O. Levy, Comput. Mater. Sci. **58**, 227 (2012).
[40]G. L. W. Hart, S. Curtarolo, T. B. Massalski, and O. Levy, Phys. Rev. X **3**, 041035 (2013).
[41]S. Curtarolo, G. L. W. Hart, M. B. Nardelli, N. Mingo, S. Sanvito, and O. Levy, Nat. Mater. **12**, 191 (2013).
[42]Y. Takagaki, A. Wirsig, M. Ramsteiner, B. Jenichen, and U. Jahn, Semicond. Sci. Technol. **29**, 075016 (2014).
[43]M. Maltseva, M. Dzero, and P. Coleman, Phys. Rev. Lett. **103**, 206402 (2009).
[44]J. Figgins and D. K. Morr, Phys. Rev. Lett. **104**, 187202 (2010).
[45]G. E. Blonder, M. Tinkham, and T. M. Klapwijk, Phys. Rev. **25**, 4515 (1982).